# Simulation of brash ice behaviour in the Gulf of Bothnia using Smoothed Particle Hydrodynamics formulation

Aniket Patil.
Researcher, PhD student
SINTEF Narvik and Luleå University of Technology, Luleå,
Rombaksveien E6-47,
8517 Narvik, NORWAY.
Email: aniket@tek.norut.no
phone: +47 48250520

Bjørnar Sand.
Senior Researcher
SINTEF Narvik,
Rombaksveien E6-47,
8517 Narvik, NORWAY.
Email: bjoernar@tek.norut.no
Phone: +47 99423525

Lennart Fransson.
Asst. Professor
Department of Civil, Environmental and Natural Resources Engineering,
Luleå University of Technology,
F983 Luleå, SWEDEN.
Email: icefrans@gmail.com
Phone: +46 920 493102

Victoria Bonath.
Research Assistant
Luleå University of Technology,
Department of Civil, Environmental and Natural Resources Engineering,
F958 Luleå, SWEDEN.
Email: victoria.bonath@ltu.se
Phone: +46 920 492934

Andrzej Cwirzen.
Professor and Head of Subject, Holder of a Chair
Luleå University of Technology,
Department of Civil, Environmental and Natural Resources Engineering,
F991 Luleå, SWEDEN.
Email: andrzej.cwirzen@ltu.se
Phone: +46 920 493387

## Abstract

The repeated passage of ships through an ice infested waters creates a field of broken ice pieces. The typical size of the broken ice pieces is generally less than 2.0 m. This area may be referred as a brash ice field. The movement of ships and vessels leads to the transportation and accumulation of broken ice pieces in brash ice field. A better understanding of the properties and behaviour of brash ice will improve the estimates of ice load associated with shipping in the brash-ice field. An in-situ test, referred here as “pull-up” test, was performed in the Luleå harbour. An attempt was made to estimate the mechanical and physical properties of brash ice field based on the in-situ test results. The test setup, procedure and test results are described in detail. Furthermore, the test is simulated using the Smoothed Particle Hydrodynamics (SPH) formulation. The purpose of the numerical simulations is to calibrate the numerical and material model of brash ice using the pull-up test measurements. In this numerical model, a discrete mass-spring-dashpot model was used to simulate buoyancy and drag. The continuous surface cap model (CSCM) was used as a material model for the brash ice. The elastic modulus and the fracture energy of brash ice as a material model input were estimated by an ad-hoc scaling formula. The parameters such as void fraction, cohesion and angle of internal friction were altered to see their influence with respect to the test data. The analysis of the in-situ test results and the simulation results provide a preliminary approach to understanding of the brash ice failure process which can be further developed into modelling techniques for marine design and operations.

Keywords: pull up test, brash ice, discrete beam element, friction coefficient.

## 1. Introduction

New shipping routes are opening across the arctic and sub-arctic areas as a result of rising temperatures and a decline in the average area of sea ice. This may increase the interest of merchant vessels to choose arctic shipping routes, see Melia et al. (2016). However, knowledge of the load levels due to the ice resistance and ice accumulation is required for safe and economic marine operations in that area. Even though the permanent sea ice cover disappears and the severity of sea ice decreases, ice features at lower concentrations will still occur. Accumulations of broken ice can pose challenges for ice engineering applications, such as rubble accumulations around structures and brash ice in ports. Each winter, ice breakers create channels to move and navigate in ice-infested waters. These channels are often covered with broken pieces of level ice, referred to as brash ice. The repeated passage of vessels in subfreezing conditions is responsible for brash ice accumulations in most channels, see Greisman (1981). Brash ice can also be found between colliding ice floes. Brash ice properties are different from the solid sea ice particularly because the brash ice is a slushy mixture of ice pieces of varying sizes. Determination of the mechanical and physical properties of brash ice is required to obtain a realistic prediction of its resistance and is therefore essential for cost-effective shipping in ice channels. Along with the additional difficulties of navigation, pressure ridges and consolidated broken ice mass, brash ice makes the Gulf of Bothnia and the Gulf of Finland one of the most challenging environments for winter navigation. The Finnish Swedish Ice Class Rules (FSICR) guide the power and strength requirements for ice-strengthened vessels operating in that area. The minimum requirement of main engine power output is dependent on ice-resistance. Some formulae for prediction of the brash ice resistance are given by Mellor (1980), Kitazawa and Ettema (1985), Ettema et al. (1986) and Ettema et al. (1998). The discrepancy between theoretically calculated brash ice resistance and that of prototype model tests, demands in situ testing which can be costly and time consuming.

The efforts are necessary to simulate a brash ice under realistic boundary conditions. Therefore, simulation of in situ or lab tests needs a numerical model which has ability to capture the brash ice behaviour under loading conditions. The brash ice is a complicated material to simulate, due to the characteristics of freezing of ice blocks together (i.e. freeze bonds) and the generally high porosity (>20%). Several numerical methods have been employed for simulation of brash ice interaction with structures, i.e.: Finite Element method (FEM), Discrete Element Method (DEM) and Smooth Particle Hydrodynamics (SPH). The discrete nature of brash ice makes the DEM more suitable for simulation of ice blocks and structure interaction where separate non-continuum elements are considered. The application of DEM to model ice rubble in ice ridges can be seen in Hopkins et al. (1991), Hopkins et al. (1999), Polojarvi and Tuhkuri (2009), Polojärvi et al. (2012) and Polojärvi and Tuhkuri (2013).

In this method, each ice block would be modelled as a particle and spherical particles are typically used for three-dimensional problems. The forces acting on each particle are then computed from the initial properties and the relevant physical laws and contact models. Sorsimo et al. (2014) have modelled a brash ice channel with discrete elements and reported a discrepancy between analytical and simulated brash ice resistance underlining the need for more experimental investigation on brash ice properties. A recent study by, Luo et al. (2020) used a numerical method by coupling CFD-DEM to study the resistance on ship by brash ice in channel. The discrete element model provides insights into complex microstructural phenomena. In the finite element method (FEM), the domain of interest is modelled with continuum elements, which gives sufficiently accurate results for small deformations, but in its conventional form is unable to simulate larger deformations. To solve this issue, Kim et al. (2019) have used finite element rigid blocks in ice-structure collision using the coupled Eulerian-Lagrangian (ALE) method. Another novel approach to simulate ship-ice interaction is given in Li et al. (2020), where they have used Extended Finite Element Method (XFEM) together with linear elastic fracture mechanics (LEFM) to simulate crack growth in ice. There has recent development in mesh-free formulation techniques such as SPH, which gives an accurate solution for large displacements that remain in continuum domain of Lagrangian framework. SPH is a fully Lagrangian method that uses meshless discretization of the computational domain, see Monaghan (2005). However, Robb et al. (2016) have used a SPH-DEM combined model to simulate river ice jams, showing the potential to combine these two methods. Cabrera (2017) have used SPH to model the experimental work of brash ice resistance on a cylinder in a tank of brash ice and implemented Mohr-Coulomb as the material model for the brash ice. They also have indicated the need for more experimental work as well as more accurate material model. Recently, Zhang et al. (2019) has used SPH to study the ice failure process in ice-ship interaction. The Drucker-Prager yield criterion was their choice of material model for ice. Since, they have not considered the effect of water in their model, SPH model overestimates the ice breaking resistance.

The SPH method, originally developed for astrophysics purposes, is basically an interpolation technique, see Gingold and Monaghan (1977) and Lucy (1977). A comprehensive review of this method is presented in Liu and Liu (2003) and Monaghan (1994). In SPH, the computational domain is discretized into a finite number of particles (or integration points). These particles carry time-history variables such as density, displacement, velocity, acceleration, strain-rate, stress-rate, act as interpolation points, and move with the material velocity according to the governing equations. The SPH formulation is preferred over the conventional finite element method due to the ability to handle large deformation. Despite gaining popularity, the main drawbacks of SPH are associated with inaccurate results near boundaries and tension instability, see Swegle et al. (1995). Also, SPH can be computationally expensive, as shown by Korzani et al. (2017). Therefore, it is very essential to find efficient problem domain sizes and to use proper boundary conditions. Table 1 summaries the numerical methods which are commonly used to simulate brash ice structure interactions.

To estimate the brash ice resistance accurately, the mechanical and physical properties of brash ice must be reliable. Many authors have indicated the gaps of material testing of brash ice and the need for suitable and robust numerical method to simulate brash ice structure interaction. The pull up test was also part of the brash ice testing campaign by Bonath et al.

(2019) and Bonath et al. (2020). The aim of this work is to not only present the results of a novel test for brash ice but also simulate the test to using SPH formulation. A brash ice field was discretised with SPH particles and used to simulate the discrete nature of brash ice. A continuous surface cap model (CSCM) was used to simulate the behaviour of brash ice. To include the buoyancy and drag due to water, ALE and CFD have been used by various researchers. Although, both approaches can give accurate solution, they can be CPU intensive and time consuming. Thus, simple approach to include the buoyancy and drag using a discrete mass-spring-dashpot element coupled to each particle is presented (details are given in section 4.1). The accuracy of the numerical model is judged based on the deformation behaviour observed in the pull-up test and the degree of fit to peak and residual forces obtained in the pull-up test. The objectives of this study were to develop a new method and practices for measuring brash ice properties and to calibrate numerical and material model using test measurement data. The Following sections provide details of the test results, numerical model, material model and finally test results and simulation results are discussed.

Table 1: Literature review of common numerical methods used to simulate brash ice structure interaction

| Numerical Method(s) | Load event / Test type | Author(s) |
|---|---|---|
| DEM | Ice resistance to ship in a channel with brash ice. | Sorsimo et al. (2014) |
| SPH-DEM Coupling | Ice accumulation upstream of an obstruction. | Robb et al. (2016) |
| SPH | Experiment of a cylinder moving thorough brash ice in a tank | Cabrera (2017) |
| SPH | Simulation of the ice failure process and ice-ship interactions | Zhang et al. (2019) |
| Coupled Eulerian-Lagrangian Method | Ship-broken ice fields interaction. | Kim et al. (2019) |
| CFD-DEM coupling | Ship-brash ice interaction process. | Luo et al. (2020) |
| XFEM | Ship ice interaction. | Li et al. (2020) |

## 2. Physical and Mechanical properties of brash ice

As defined by Weeks (2010), brash ice is an accumulation of floating ice made up of fragments not more than 2 m across (small ice cakes), the remnants of other forms of ice. But in a brash ice-covered ship channel the ice piece size rarely exceeds 1 m, due to frequent ice breaking operations. During wintertime, ice channels are made by ice breakers to allow ships to navigate and access port areas. If undisturbed the ice blocks tend to refreeze at the surface due to sub-zero air temperature. Thus, it becomes necessary to rebreak the channel to maintain accessibility. However, Greisman (1981) points out that frequent passage to rebreak the channel to keep it unconsolidated can enhance the rate of accretion. Ice pieces are pushed asides during the ice breaking process, forming a ridge-like structure, see Greisman (1981) and Sandkvist (1978). This leads to more lateral confinement. This lateral restraining force is essential to balance the hydrostatic and gravity forces which tend to act to spread the pieces to a uniform layer thickness. The cross-section of the brash ice channel is typically thickest at the channel edge and thinnest in the middle. In this respect, the brash ice channel differs somewhat from a brash ice field. The ice pieces in the brash ice field are uniformly distributed and can be spread across several square kilometre. Depending on the lateral confinement or constraint, layers of blocks are stacked on top of each other. Absence of any lateral confinement will make all blocks floating at same level. A typical brash-ice field profile is shown in Fig. 1. In the brash ice field, voids between blocks are filled with water or air, depending on their position relative to the water level. The ice blocks may be rounded or become spherical, because of repeated passage. If the ice blocks are not refrozen, brash-ice field does not have freeze bonds, and hence has no tensile strength. However, the resistance created by the floating broken ice pieces is higher than the open water. Some ships have difficulty moving through this broken ice mass even though there is no significant cohesion between those ice pieces. This is a common occurrence in port areas and brash ice channels. Formation, growth and accumulation of the brash ice depend on several factors including air temperature, channel passage frequency, ice block shape and size, initial confinement conditions of the blocks and the strength and form of the freeze bonds, see Mellor (1980) and Riska et al. (2019). However, the strength of freeze bonds between ice blocks is influenced by confinement pressure, contact time and area, and salinity of the water in which bonding, or fusion, occurs, see Ettema et al. (1998). The brash ice does not behave in a mechanically similar manner as the level ice. It can impede vessel motion and trap low powered vessels. The brash ice resistance is different from that of level ice. Based on some similarities between coarse-grained soil and brash ice, it is possible to characterise the brash ice as a Mohr-Coulomb solid. The behaviour brash ice can be represented by Mohr-Coulomb yield criterion, due to large deformations and compaction under normal loading characteristics see Kitazawa and Ettema (1985) and Matala and Skogström (2019). Greisman (1981) suggest that below a critical strain rate or ship speed the brash ice behaves as a cohesive friction material. Above this speed, fluidization of the medium occurs, and the resistance can be approximated to a viscous, laminar fluid.

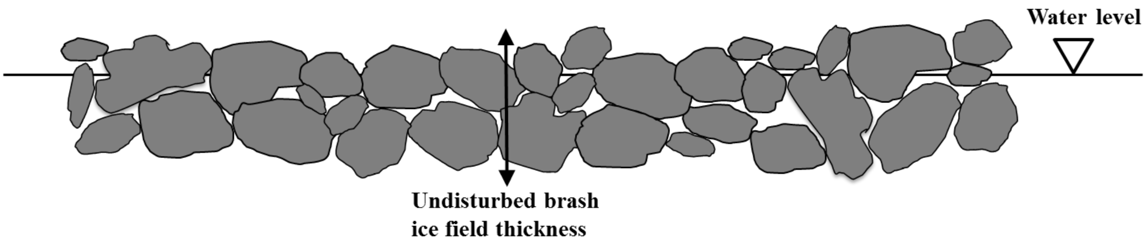


Fig. 1. Typical cross section of brash-ice field

The compressive strength of ice pieces is an ultimate limiting factor when estimating the brash ice resistance. The brash ice resistance to shearing increases with the confinement pressure. The stresses involved in the brash ice resistance problem are relatively low so that a linear Mohr-Coulomb criterion has been suggested by ISO19906 (2010) and Trafi (2010) to give upper load levels. Thus, the major requirement for material modelling of brash ice is associated with finding accurate values of the angle of internal friction $(\phi)$ together with corresponding values of the unconfined shear strength or cohesion, $(c)$. Several tests have been done in laboratory and in-situ, to understand the behaviour and failure mechanics of brash ice. In literature, values of angle of internal friction $(\phi)$ranging from 42° to 58° are reported, see Tatinclaux et al. (1976), Keinonen and Nyman (1978), Prodanovic (1979) and Fransson and Sandkvist (1985). The higher values of angle of internal friction are from results with no or negligible tensile strength. The cohesive strength comes from consolidation of ice blocks. The thermal condition and confinement pressure or normal load are the main factors controlling the cohesive strength. When the external force is applied to brash ice, rearrangement of ice pieces leads to denser packing. This property of brash ice is called compressibility. Further increase in external force may lead to the breaking of ice pieces depending on degree confinement. The linear Mohr-Coulomb criterion overestimates the load levels of brash ice as it does not take compressibility into account. One way to characterize this behaviour in material model is to place a limit (i.e. cap) on the compression side and allow it to grow or shrink based on loading.

Ice resistance to ships sailing in brash ice channels has been investigated theoretically and experimentally by Keinonen and Nyman (1978), Mellor (1980), Kitazawa and Ettema (1985), Ettema et al. (1998), Hu and Zhou (2015), Jeong et al. (2017) and Dobrodeev and Sazonov (2019). One of the important factors in navigating through brash ice channels is frictional resistance between ice blocks and ship’s hull. While going through the channel, each vessel passage moves, rolls and grinds the individual ice blocks against one another and the ship's hull. According to Ettema et al. (1986), the total resistance to ship hull motion in brash ice channel is sum of separate resistance components. These components are generally associated with the shearing or compression of brash ice layer, rearrangement and/or movement of ice blocks and friction between the ship hull and ice blocks. These resistance terms are interdependent. For example, compaction of ice blocks by hull increases confinement of nearby ice blocks which leads to higher ice to ice frictional resistance. Tatinclaux et al. (1976) concluded in their experiment of pushing a vertical plate through the ice, that the crushing resistance was inversely proportional to the pushing speed and the resistance was also apparently insensitive to the shape of the ice blocks. Dobrodeev and Sazonov (2019) have shown that the ice to hull friction coefficient has a minimal effect on the resistance magnitude.  Most of the ice blocks in brash ice channel are either completely or partially submerged in water. Therefore, this is primarily a "wet" friction process. Furthermore, the frictional force decreases with increasing void fraction due to the corresponding decrease in confinement and contact area. Various authors including Fransson and Sandkvist (1985) and Sukhorukov and Løset (2013) reported friction coefficients as low as 0.01 for the wet friction process.

## 3. Test setup and results

The location of test site was in a vast area of brash ice field at Luleå harbour. The tests were conducted using novel equipment fabricated in-house. The test equipment consists of a nylon net supported by an octagonal structure (which has a closing and locking mechanism) resembling an upside-down umbrella and hereafter is referred to as the collector. The collector has eight arms which are connected at the central hub and the hub is then joined to a pole. (See Fig. 2). The pole is connected to an on-board crane of a tugboat. Before starting the test, the collector was lowered into the brash ice. The weight of the collector enabled relatively easy penetration of the ice. Moreover, the arms of the collector were folded to an acute angle during entry then unfolded under the brash ice. and pulled up vertically until completely lifted above the water. A load cell, placed between the pole and the crane, was used to record the force-time graph. The ship crane was to lower and pull up the collector with almost constant velocity.

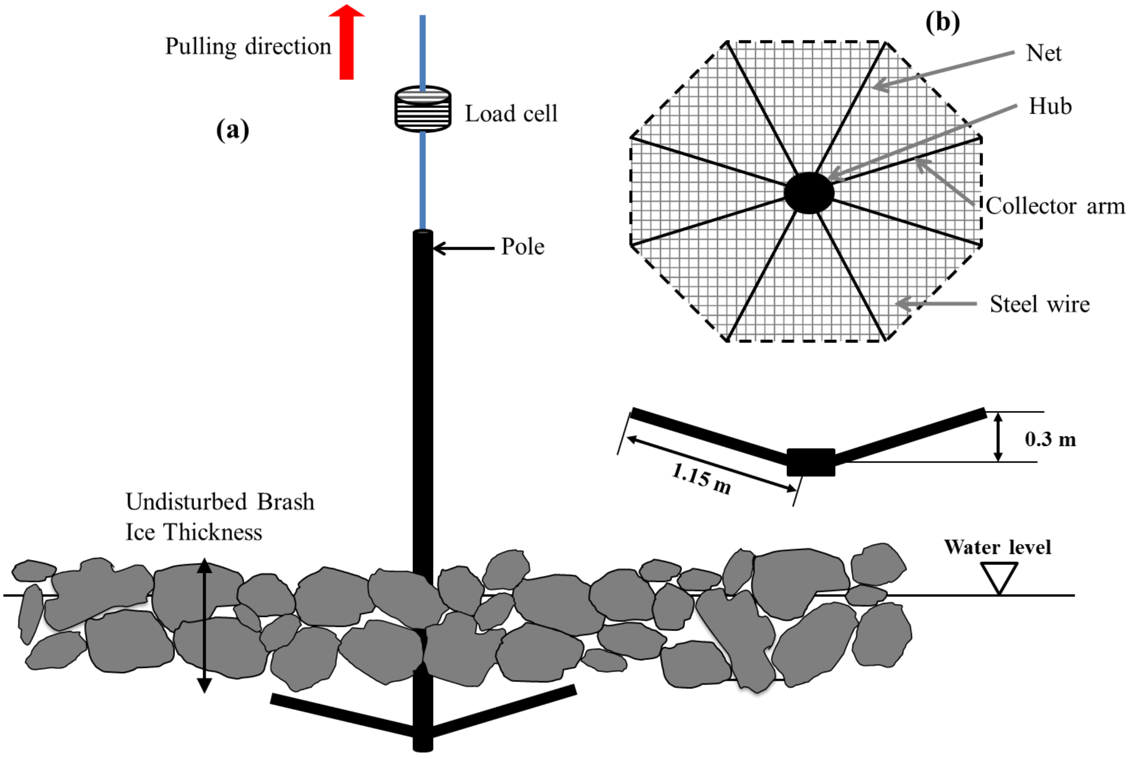


Fig. 2. (a) Schematic of the pull-up test (b) Parts of the collector.

The underlaying assumption of the test was that the collector will left (pull up) the ice blocks out of water and doing so ice resistance to deform will be registered. Due to bad weather and faulty folding mechanism several unsuccessful attempts were made to get reasonable data. In this study a single test data was selected to further investigation. The force-time graph corresponding to selected test is shown in Fig. 3 where initial stage denoted by 1 reveals the contact between the collector and the ice, before the start of the test. Then, collector was pulled up with fairly constant velocity which results in a fast increase in the force, up to the peak denoted by (2). A subsequent peak denoted by (3) in Fig. 3, which occurs after 58 sec of testing, is attributed to the rearrangement of ice blocks. After the second peak, the force declined and remained constant. The force decreased slightly due to the falling of small pieces of ice and draining of water. Subsequently, the force decreases to a constant level, denoted by (4), indicating all water was drained out. Now, this load level represents the dry weight of ice pieces hanging in the collector. It is to be observed that the low point between (2) and (3) that is greater than (4).

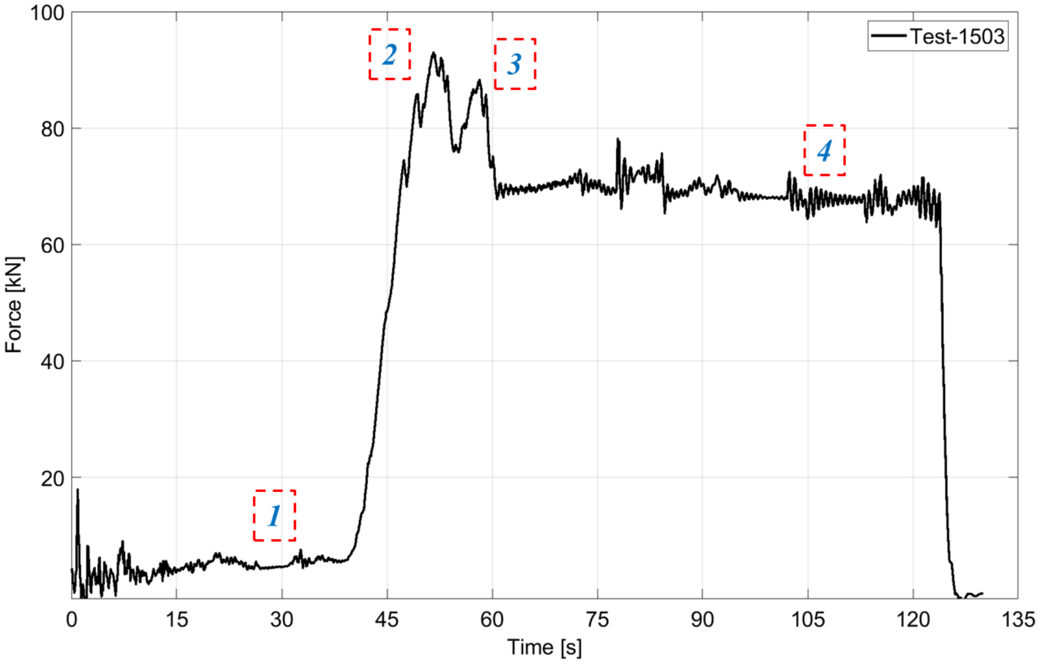


Fig. 3. Force-time plot for pull up tests.

The force required to lift the collector out of the water can be decomposed (see Fig. 4) into the following components: (i) The frictional force $(F_f)$ arises from the interaction between loose blocks. (ii) The effective force acting on the brash ice blocks due to gravity $(F_g)$ and buoyancy $(F_b)$. Therefore, in this scenario, ice blocks interact with each other and the load applied to one block is transmitted by contact forces developed between adjacent blocks.

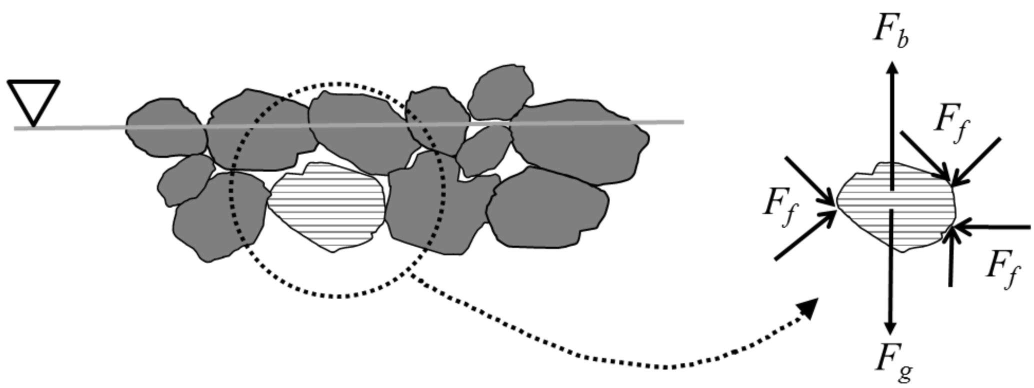


Fig. 4. Decomposition of forces on an ice block

The frictional contact forces $\left(F_f\right)$ can be further divided into normal and tangential components as shown in Fig. 4. The tangential force component depends on the normal force. These force components depend on the shape and size of blocks and the existence of freeze bonds. Thus, the effective force can be registered as the summation of gravity, buoyancy and friction forces in the absence of freeze-bonding.

Table 2: Environmental parameters

| **Parameter** | **Symbol [unit]** | **Value** |
|---|---|---|
| Temperature of water | $T_w$ [°*C*] | *0* |
| Temperature of ice | $T_i$ [°*C*] | *-1* |
| Temperature of air | $T_a$ [°*C*] | *-1* |
| Salinity | *S* [ppt] | *0.3* |
| Undisturbed thickness of the brash ice | $h_i$ [m] | 1.2 |

The undisturbed thickness of the brash ice and other environmental parameters were measured and are listed in Table 2. The measurement accuracy is limited due to the human factor, because some of the measurements were taken manually. As the collector moves upward, deformation starts at the bottom, thereby resulting in the upward movement of the ice blocks and the formation of a failure plane. At the beginning of pulling, a wider area than collector was moved, resulting in the formation of an upward conical-type plug. The conical-type plug, which is a result of the interlocking of the blocks, becomes more cylindrical with the upward movement of the collector. Pieces at the edges of this plug start falling as soon as this plug comes out of the water. The plug formed at the end of the test is shown in Fig. 5.

(a) Plug formed after collector is completely removed from the water and is hanging in the air

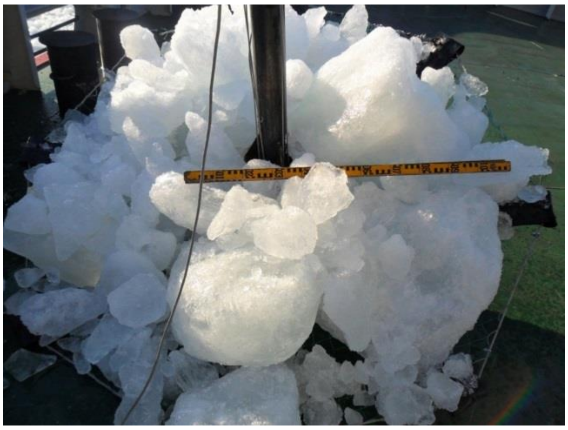

(b) Ice blocks collected by the collector after the test

Fig. 5. Photos of test

Based on a video clip and the force-time plot shown in Fig. 3, approximately 20 seconds were needed to move the collector from the ice bottom to the water surface.

## 4. Numerical model of pull-up test

The pull-up test was simulated using SPH formulation and CSCM as material model for brash ice. LS-DYNA a general-purpose multi-physics explicit finite element analysis code was used. Moreover, a parametric study was conducted via massively parallel processing (MPP) where 8 (eight) separate CPUs were run in parallel. A finite dimensioned, 3D brash ice field was generated with specially written code in MATLAB 2018b. The SPH elements were created with solid centre method with 100% fill, which means a SPH element with 100 % mass. The particle renormalization approximation theory and the default smoothing length were used for all simulations, see LS-DYNAa (2017). For a theoretical explanation of SPH implementation in LS-DYNA please refer to Tran (2018), Yreux (2018), Patil et al. (2015) and Xu and Wang (2014). A snapshot at t=0 of the numerical model in Z-X plane showing SPH particles, the collector and the pole, is given in Fig. 6.

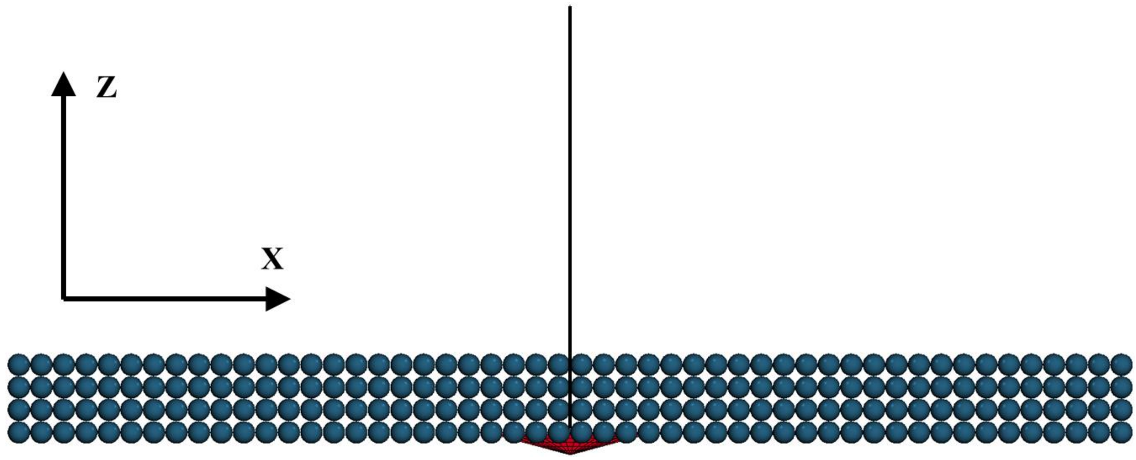


Fig. 6. Numerical model at the start of the test.

As the ice block size distribution were not measured in current test, the SPH particle size is chosen as representative of ice block size. The uniform particle spacing was used to discretise the geometry of the brash ice field. The buoyancy force on each particle was simulated by the mass-spring-dashpot model. The workings of mass-spring-dashpot model are described in section 4.1. The overall size of the numerical model was kept large enough to ensure that boundary conditions of numerical model of brash ice field did not affect the simulation results. Table 3 gives particle spacing and model size dimensions. Moreover, particles at the edge of the brash ice model were fixed in all directions and thereby restrained. The collector was modelled with shell elements of rigid material based on the assumption that the collector resists any deformation. The pole was discretized with eight beam elements in length direction. The top node of top beam element was pulled with constant velocity in the Z direction ($V$=0.052 m/s). It was fixed in the other two (i.e. X and Y) directions and all rotational degrees of freedom are constrained. These boundary conditions give same movement of the pole as was observed in field test. As suggested by Mellor (1980), if the thickness of brash ice ($h_i$) is significantly greater than the average ice block size ($t$), lateral confinement of the layer must be assumed for cohesionless brash ice,. otherwise, ice blocks would spread out until the layer becomes one ice block thick. In the absence of externally applied forces or displacements, the internal stresses in the brash ice field are induced by gravity, buoyancy and frictional forces, see Fig. 4. To give lateral confinement, all the SPH particles at the edge of numerical brash ice field are fixed in all direction. Table 3 gives the numerical model geometrical parameters.

Table 3: Numerical model geometrical parameters

| Parameter | Symbol [unit] | Value |
|---|---|---|
| Length of brash ice field in x, y direction | $L_x$, $L_y$ [m] | 15 |
| Thickness of brash ice field z direction<br>*(i.e. undisturbed brash ice field thickness)* | $L_z$ [m] | 1.2 |
| SPH particle spacing in x, y and z direction | $l_x$, $l_y$, $l_z$ [m] | 0.3 |

Following assumptions were made in the numerical model of brash ice field:

1. All material properties were considered constant throughout the brash ice field.
2. The temperature of ice blocks in the brash ice field was considered constant.
3. The pole and collector were considered being rigid bodies.

### 4.1. Buoyancy and hydrodynamic forces

In the present study buoyancy and drag forces are included in the numerical model using a discrete mass-spring-dashpot model. The buoyancy and drag on the brash ice field was simulated by using finite length beam elements. In this setup, each SPH particle was then connected to a discrete mass-spring-dashpot model, see Fig. 7 (a). Also, a simple drag model was added to the spring element equation (see eq. 3). The total force $F_{T,i}$ for the mass-spring-dashpot system in global Z-direction is given as

$$F_{T,i} = F_{b,i} + F_{d,i} + \rho_i (1 - V_f) g l_x l_y l_z \tag{1}$$

Where, $F_{b,i}$ and $F_{d,i}$ are the buoyancy and drag forces acting on each SPH particle, g is the acceleration of gravity, $\rho_i$ is density of ice and $V_f$ is the void fraction.

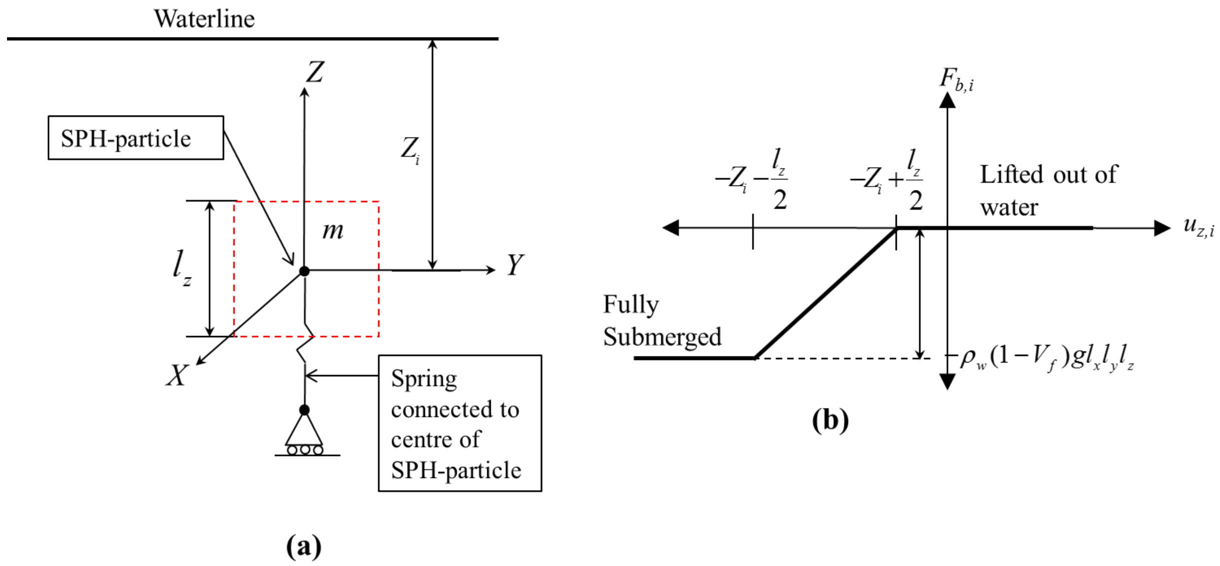


Fig. 7. (a) Mass-spring-dashpot model for SPH Particle. (b) The force vs. displacement diagram for springs attached to SPH.

The buoyancy force $F_{b,i}$ is function of the displacement $u_{Z,i}$, relative to the waterline as shown in Fig. 7 (b) and is expressed as:

$$F_{b,i} = \begin{cases} 0 & u_{z,i} \geq -Z_i + \frac{l_z}{2} \\ -\rho_W(1-V_f)gl_xl_y\left(u_{z,i} + Z_i - \frac{l_z}{2}\right) & -Z_i - \frac{l_z}{2} \leq u_{z,i} \leq -Z_i + \frac{l_z}{2} \\ -\rho_W(1-V_f)gl_xl_yl_z & u_{z,i} \leq -Z_i - \frac{l_z}{2} \end{cases} \quad (2)$$

Where $\rho_W$ is density of the water. The drag force $F_{d,i}$ can be estimated by a basic viscous damping equation for an object moving with a vertical velocity $\dot{u}_{z,i}$ through a liquid:

$$F_{d,i} = \frac{1}{2}\dot{u}_{z,i}{}^2 C_d \rho_W (1-V_f) l_x l_y \quad (3)$$

Where $C_d$ is the drag coefficient. In all simulations, the value of the drag coefficient $C_d = 1.05$ was used, i.e. assuming the shape of a cube moving through a fluid.

A penalty-based, node-to-surface contact formulation is employed for simulating contact between SPH particles and the collector. In LS-DYNA, the frictional coefficient, $\mu$ is assumed to be dependent on the relative velocity $V_{rel}$ of the nodes and surfaces in contact and calculated as follows

$$\mu = \mu_D + (\mu_S - \mu_D)e^{\left(-D_c|V_{rel}|\right)} \tag{4}$$

Where, $\mu_s$, $\mu_D$ and $D_C$ are the static, dynamic and exponential decay coefficient of friction, respectively. To model the ice to collector friction, the values of 0.57, 0.06 and 0.02 were chosen for static, dynamic and decay coefficient, respectively.

## 5. Estimation and scaling of material model parameters

As mentioned earlier, the material model used for brash ice was a continuous surface cap model (CSCM). The CSCM was developed by Schwer and Murray (1994) and implemented by Schwer and Murray (2002). The CSCM was also used to simulate the behaviour of ice rubble in the keel part of a first year ridge in punch through test by Patil et al. (2015). The CSCM requires a relatively large number of input parameters. Based on test results from pull-up tests, described herein, some of the necessary input data to simulation can be estimated. But the material model parameters required for input for the CSCM, cannot be obtained directly in the current test set up. Thus, assumptions were made regarding shear surface, cap surface and damage parameters. Later a parametric study was conducted to find the values of these parameters that gave the best fit to the test data.

Like any other granular material, the void fraction has a significant effect on material properties of brash ice. The void fraction of brash ice affects buoyancy, compressibility and the contact area between the interacting structure and the ice blocks. In the pull-up test, void fraction also affects dry brash ice weight directly. As the void fraction of brash ice in the pull-up test was not measured, an estimation is needed. One can estimate the void fraction of brash ice in the test by measuring the dry brash ice weight divided by the gross volume of the ice blocks of varying sizes. That estimate would not be accurate as many of blocks have fallen off the collector thus decreasing the actual control volume. Bonath et al. (2019) have conducted similar tests, obtaining void fraction values ranging from 57% to 77%, which were high compared to other values reported in various literature. Thus, due to uncertainties in the estimation, parametric analyses were conducted to study the effect of the void fraction.

The mechanical properties of brash ice depended on the properties of parent ice sheet. According to Fransson and Stehn (1993), most of porosity in low saline ice originates from trapped air and the strength of warm ice decreases proportionally with increase in porosity. Therefore, as a preliminary approach, properties of parent ice sheet were scaled by factor of $\left(1-\sqrt{V_f}\right)$ to obtain the properties of brash ice. A scaling formula was used to estimate the effective elastic modulus $E_{br}$, which is based on the void fraction $V_f$, see eq. 5.

$$E_{br} = E_{ice}\left(1-\sqrt{V_f}\right) \tag{5}$$

Where $E_{ice}$ is elastic modulus of parent level ice. Then, following relationships were used to calculate the Bulk modulus $K_{br}$ and Shear modulus $G_{br}$, see eq.6.

$$G_{br} = \frac{E_{br}}{2(1+\upsilon)}, K_{br} = \frac{E_{br}}{3(1-2\upsilon)} \tag{6}$$

The brash ice behaviour was modelled using a continuous surface cap model (CSCM) which is proposed by Sandler et al. (1976). A detailed theoretical description and comprehensive calibration procedure of CSCM is given in Murray (2007) and Murray et al. (2007). The CSCM model combines the shear failure surface with cap hardening surface compaction smoothly and continuously by using a multiplicative formulation. The multiplicative formulation is used to combine the shear failure surface with the isotropic hardening compaction cap surface smoothly and continuously, thus avoiding any numerical instability associated. The general shape of the yield surface in meridional plane is shown in Fig. 8.

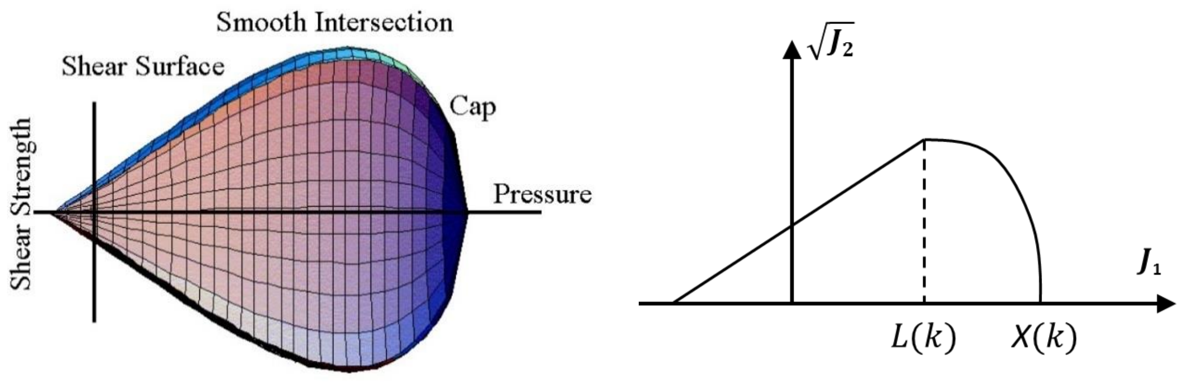


**(a)** **(b)**

Fig. 8. General shape of the CSCM model yield surface in meridional plane (from Murray et al. (2007)). (b) Single smooth cap failure function (from Schwer and Murray (1994))

The failure surface of the smooth cap model is defined as

$$F_f(J_1) = \alpha - \lambda \exp^{-\beta J_1} + \theta J_1 \tag{7}$$

where $J_1$ is the first invariant of the deviatoric stress tensor and *α, θ, λ*, and *β* are model parameters used to match the triaxial compression. The isotropic hardening or cap surface of the model is based on a non-dimensional functional form, given below

$$F_c(J_1, \kappa) = 1 - \frac{[J_1 - L(\kappa)].[|J_1 - L(\kappa)| + J_1 - L(\kappa)]}{2[X(\kappa) - L(\kappa)]^2}. \tag{8}$$

Where, $\kappa$ is a hardening parameter that controls the motion of the cap surface. $L(\kappa)$ and $X(\kappa)$ define the geometry of the cap surface. The smooth cap model, shown in Fig. 8 (a), is formed by multiplying together the failure and hardening surface functions to form a smoothly varying function given by

$$f(J_1, J_2^{'}, \kappa) = J_2^{'} - F_f^2.F_C. \tag{9}$$

Where $J_2'$ is the second invariant of the deviatoric stress tensor. The CSCM parameters can be divided into three categories: yield surface parameters, cap parameters and damage parameters. To define the yield surface, triaxial material model parameters, *α, θ, λ* and *β* which can be estimated by fitting to triaxial experimental data. Due to absence of such experimental data, the triaxial compression parameters such as $\alpha$ and $\theta$ were calculated based on relationship (see eq. 10) given by Schwer and Murray (1994) to Mohr- Coulomb surface.

$$\alpha = \frac{6c\cos\phi}{\sqrt{3}(3-\sin\phi)}, \theta = \frac{2\sin\phi}{\sqrt{3}(3-\sin\phi)} \tag{10}$$

Where $c$ is the cohesion and $\phi$ is the angle of internal friction. As per the recommendation of Murray (2007), other yield surface parameters are defined based on tri-axial compression ($\lambda$, $\beta$), deviatoric state of torsion ($\alpha_1$ $\theta_1$, $\lambda_1$ and $\beta_1$) and tri-axial extension ($\alpha_2$, $\theta_2$, $\lambda_2$ and $\beta_2$). This ensures a smooth transition between the tensile and compressive pressure regions. the following values were used in all simulation, see eq. 11.

$$\begin{aligned} &\lambda = 0,\ \beta = 0, \\ &\alpha 1 = 0.7373,\ \theta 1 = 0,\ \lambda 1 = 0.17,\ \beta 1 = 0, \\ &\alpha 2 = 0.66,\ \theta 2 = 0,\ \lambda 2 = 0.16, \beta 2 = 0 \end{aligned} \tag{11}$$

The cap moves to simulate plastic volume change. The cap expands ($X(\kappa)$ and κ increase) to simulate plastic volume compaction and the cap contracts ($X(\kappa)$ and $\kappa$ decrease) to simulate plastic volume expansion, called dilation (see Fig. 8). The motion (expansion and contraction) of the cap is based on the cap hardening function, as given in eq. 12.

$$\varepsilon_v^P = W(1 - e^{-D_1(X_1 - X_0) - D_2(X_1 - X_0)^2}) \tag{12}$$

Where $\varepsilon_v^P$ is the plastic volumetric strain, $W$ is the maximum plastic volumetric strain, $X_0$ is the initial intercept of the cap surface, $R$ is cap aspect ratio and $D_1$ and $D_2$ are the linear and quadratic shape parameters respectively. The five input parameters ($X_0$, $W$, $D_1$, $D_2$, and $R$) are needed to define the cap surface. Heinonen (2004) has used a hardening rule to calibrate the Drucker-Prager cap model based on a punch though test for first year ice rubble. As a preliminary approach, due to the similarities between first year ice rubble and brash ice, the cap hardening parameters in CSCM were chosen in such a way that a fit was obtained to the hardening function defined by Heinonen (2004). The comparison between the pressure-volumetric strain curves of simulation B-1 (see Table 6) based on eq. 12 and to that of hardening function defined by Heinonen (2004), is given in Fig. 9.

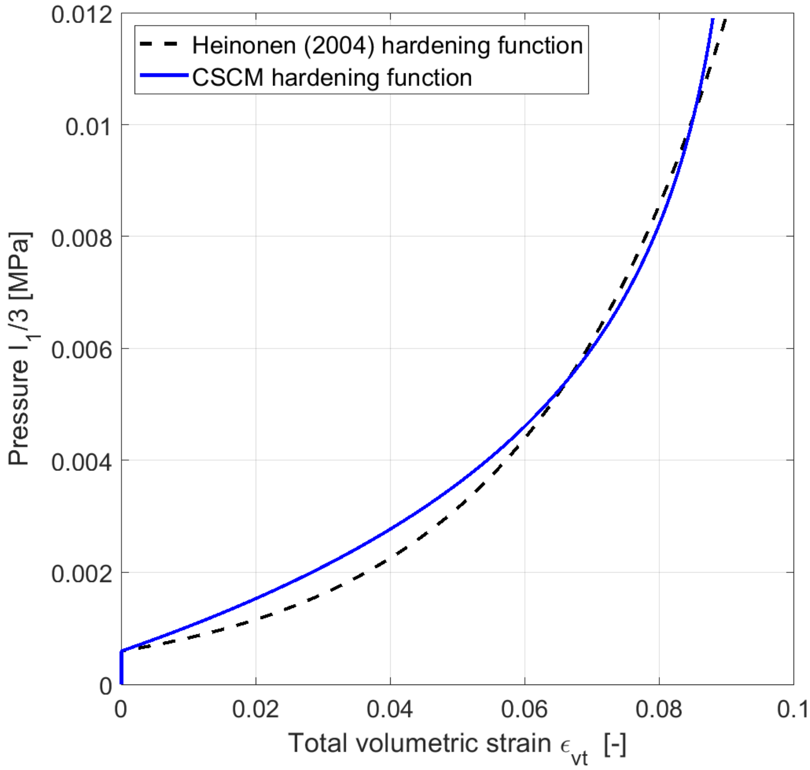


Fig. 9. Comparison of hardening function

The damage formulation is based on the work of Simo and Ju (1987) and Murray et al. (2007). Two main types of damage are included in CSCM; 1) Ductile damage that degrades stress when the mean stress is compressive, and 2) Brittle damage that degrades stress when the mean stress is tensile. The damage parameter is used to degrade the undamaged stress. The mesh size sensitivity is regulated by maintaining constant fracture energy regardless of the element size. This is done by including the element length, $L$ (cube root of the element volume), a fracture energy type term $\left(G_f\right)$ and softening parameters. The detailed formulation can be found in Murray (2007). Three types of fracture energies and two softening parameters are needed as user input, see Table 7 for input values. The fracture energy $G^C_{f,br}$ for the brash ice in uniaxial compression was scaled based on void fraction and calculated with eq. 13.

$$G^C_{f,br} = G^C_f\left(1-\sqrt{V_f}\right) \tag{13}$$

Where, $G_f^C$ is the fracture energy in uniaxial compression for parent level ice. Similarly, fracture toughness for brash ice $K_{I,br}^C$, was also scaled based on the reference fracture toughness $K_I^C$ by using a void fraction, see eq. 14.

$$K_{I,br}^C = K_I^C\left(1-\sqrt{V_f}\right) \tag{14}$$

The fracture energy in uniaxial tension $G_{ft,br}$ and in pure shear $G_{fs,br}$ stress state are treated as identical and calculated as follows, see eq. 15.

$$G_{ft,br} = G_{fs,br} = \frac{\left(1-\nu^2\right)K_{ic,br}{}^2}{E_{br}} \tag{15}$$

Table 4 gives the parent ice sheet properties used in the material model parameter calculations.

Table 4. Base value for material model input estimation

| Parameter | Symbol [unit] | Value |
|---|---|---|
| Poisson's ratio | $\nu$ [-] | 0.3 |
| Density of ice | $\rho_{ice}$ $\left[kg/m^2\right]$ | 900 |
| Elastic modulus of level ice | $E_{ice}\left[MPa\right]$ | 4000 |
| Fracture toughness of reference level ice | $K_I^C\,[\,kPa\sqrt{m}\,]$ | 100 |
| Fracture energy of reference level ice in compression | $G_f^C\left[MPa-mm\right]$ | 2.0E-05 |

The shear surface constant term in compression $(\alpha)$ and the shear surface linear term in compression $(\theta)$ were calculated based on the relationship to cohesion$(c)$ and internal fraction angle $(\phi)$, as given by eq. 10. In all simulations only one parameter was varied while others are kept constant. Table 5 gives summery of simplified input to parametric study in terms of Mohr-Coulomb strength parameters i.e. cohesion $(c)$ and angle of internal friction $(\phi)$. The CSCM parameters input is given in Table 6 and Table 7. Please note that all the values are in a consistent system of units required for LS-DYNA.

Table 5. Simplified input to the parametric study (add Sy

| Variables \ Simulation No. | A-1 | A-2 | A-3 | B-1 | B-2 | B-3 | B-4 | B-5 | C-1 | D-1 |
|---|---|---|---|---|---|---|---|---|---|---|
| Void fraction, ($V_f$)[%] | 70 | 70 | 70 | 60 | 60 | 60 | 60 | 60 | 50 | 36 |
| Cohesion $(c)$ [kPa] | 0.2 | 0.05 | 1 | 0.2 | 0.05 | 1 | 0.2 | 0.2 | 0.2 | 0.2 |
| Angle of internal friction $(\phi)$ [°] | 50 | 50 | 50 | 50 | 50 | 50 | 40 | 60 | 50 | 50 |

Table 6: The shear surface parameters ($\alpha$ & $\Theta$) and cap surface parameters for all simulations

| **Name of variable** | **Symbol [unit]** | **A-1, B-1, C-1, D-1** | **A-2, B-2** | **A-3, B-3** | **B-4** | **B-5** |
|---|---|---|---|---|---|---|
| Shear surface constant term (compression) | $\alpha$ [MPa] | 2.0E-04 | 1.0E-04 | 1.0E-03 | 2.0E-04 | 2.0E-04 |
| Shear surface linear term (compression) | $\theta$ [rad] | 0.396 | 0.396 | 0.396 | 0.315 | 0.469 |
| Cap aspect ratio | $R$ [-] | 8.957 | 8.957 | 8.957 | 17.205 | 8.957 |
| Cap initial location | $X_0$ [MPa] | 0.002 | 4.5E-04 | 0.009 | 0.004 | 0.004 |
| Maximum plastic volume compaction | $W$ [-] | 0.093 | 0.093 | 0.093 | 0.093 | 0.093 |
| Linear shape parameter | $D_1$ [-] | 86 | 386 | 23 | 43 | 386 |
| Quadratic shape parameter | $D_2$ [-] | 0.030 | 0.030 | 0.030 | 0.030 | 0.030 |

Table 7: The damage parameters for all simulations

| **Name of variable** | **Symbol [unit]** | **A-1, A-2, A-3** | **B-1, B-2, B-3, B-4, B-5** | **C-1** | **D-1** |
|---|---|---|---|---|---|
| Ductile shape softening parameter | B [-] | 1 | 1 | 1 | 1 |
| Fracture energy in uniaxial Compression | $G_{fc,br}$ $[MPa-mm]$ | 3.27E-03 | 4.51E-03 | 5.86E-03 | 8.00E-03 |
| Brittle shape softening parameter | D [-] | 1 | 1 | 1 | 1 |
| Fracture energy in uniaxial tension | $G_{ft,br}$ $[MPa-mm]$ | 3.72E-04 | 5.13E-04 | 6.66E-04 | 9.10E-04 |
| Fracture energy in pure shear stress | $G_{ts,br}$ $[MPa-mm]$ | 3.72E-04 | 5.13E-04 | 6.66E-04 | 9.10E-04 |

## 6. Analysis of Numerical Simulation Results

The stage encompassing *t*=40 to 80 seconds of the test was selected for the simulations, since the lifting of ice mass started at about *t*=40 sec, see Fig. 3. The void fraction, cohesive strength and angle of internal friction were the variables in this parametric study. The values of these variables were selected with ad hoc approach (see Table 5). The influence of each variable on the simulated force-time graph in comparison with a measured force-time graph can be seen in Fig. 10 to Fig. 13. The influence of void fraction in brash ice on the simulations results is compared with the test results in Fig. 10.

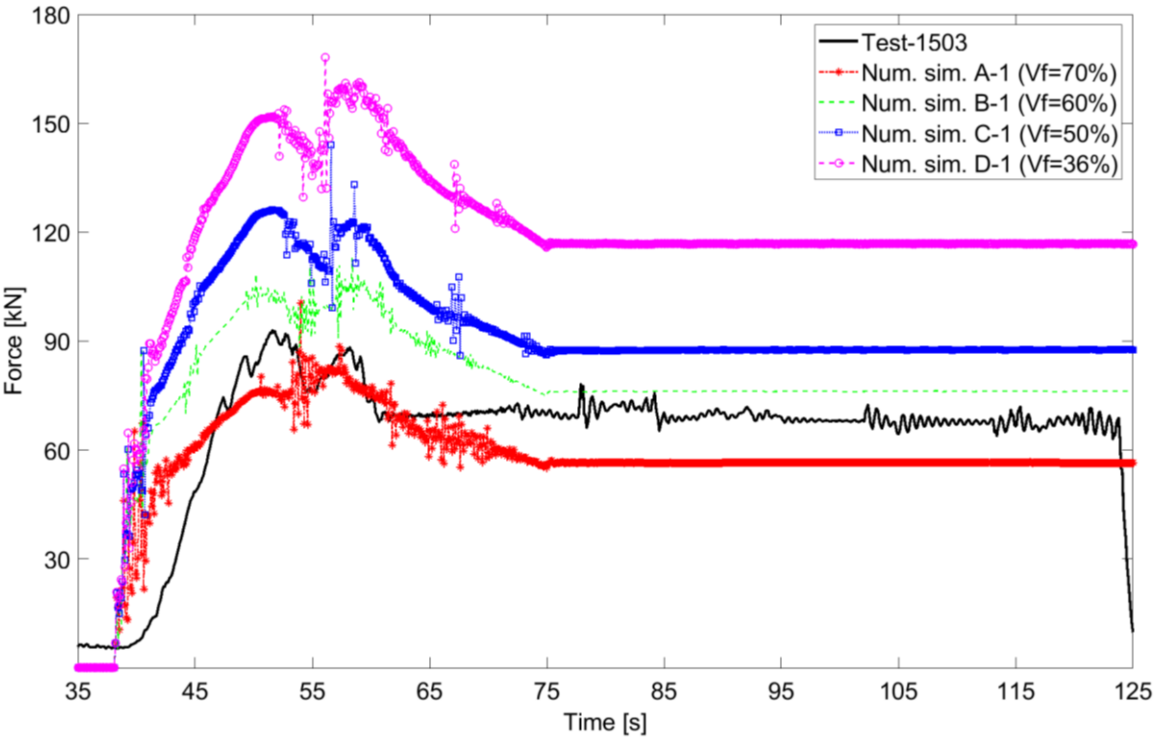


Fig. 10. Comparison of void fraction ($V_f$) (c=0.2kPa, φ=50°)

The simulation A-1 with 70% void fraction has a peak force closer to measured peak force but gives lower residual force. The simulation B-1 which has 60% void fraction gives residual force close to that of the measured results. However, the peak force for this simulation is somewhat higher than that of measured. The other two simulations C-1 and D-1 have much higher peak force and residual force values. The simulation D-1 registered the higher force of all, due to the high density of the lifted volume of brash ice. The influence of friction angle $(\phi)$ and cohesion $(c)$ were compared for void fraction 60% in Fig. 11 and Fig. 13 respectively. The variation in angle of internal friction did not give a significant change in peak force and residual force, see Fig. 11. This indicates that the major component of force was shear strength. But the difference can be seen between the initial part of numerical simulation curves, indicative of breakage of initial cohesion to form a plug.

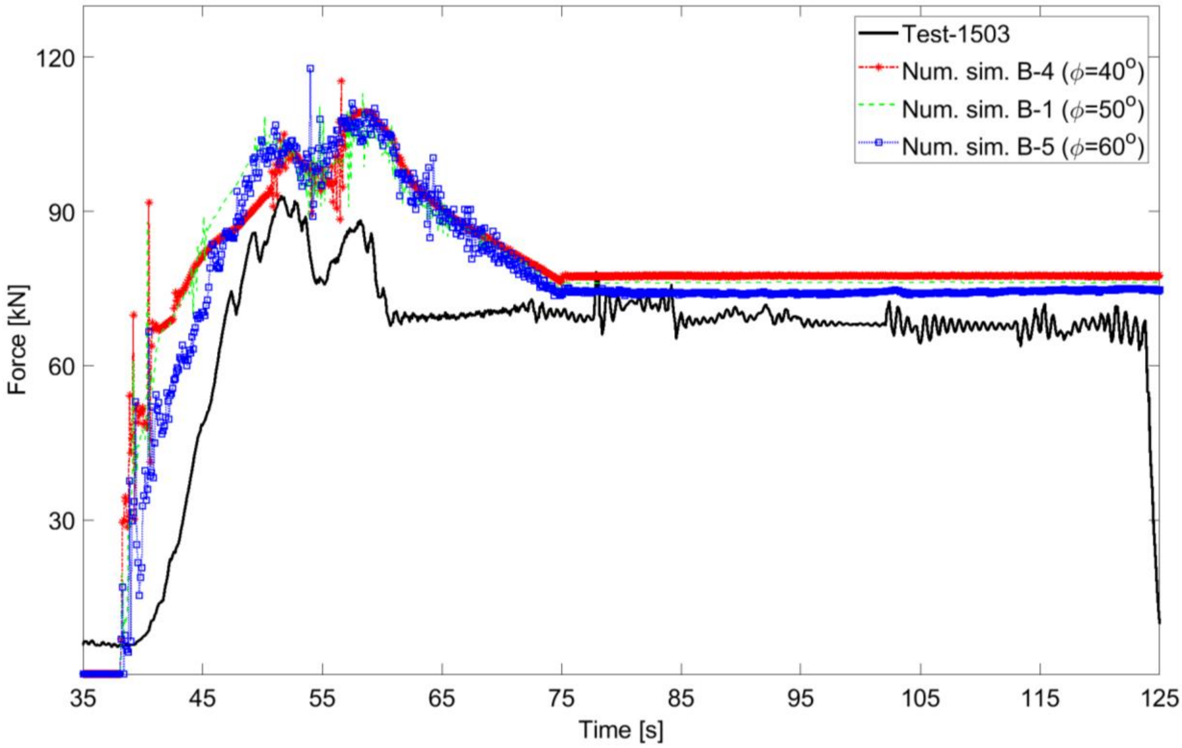


Fig. 11. Comparison of Friction angle (φ) ($V_f$=60%, c=0.2kPa)

The cohesion values were altered to examine their influence with respect to the measured force time history, see Fig. 12 and Fig. 13. The simulation series "A" has 70 % void fraction and "B" has 60% void fraction. In simulations A-1, A-2 and A-3 cohesion values of 0.2kPa, 0.05kPa and 1kPa were used respectively.

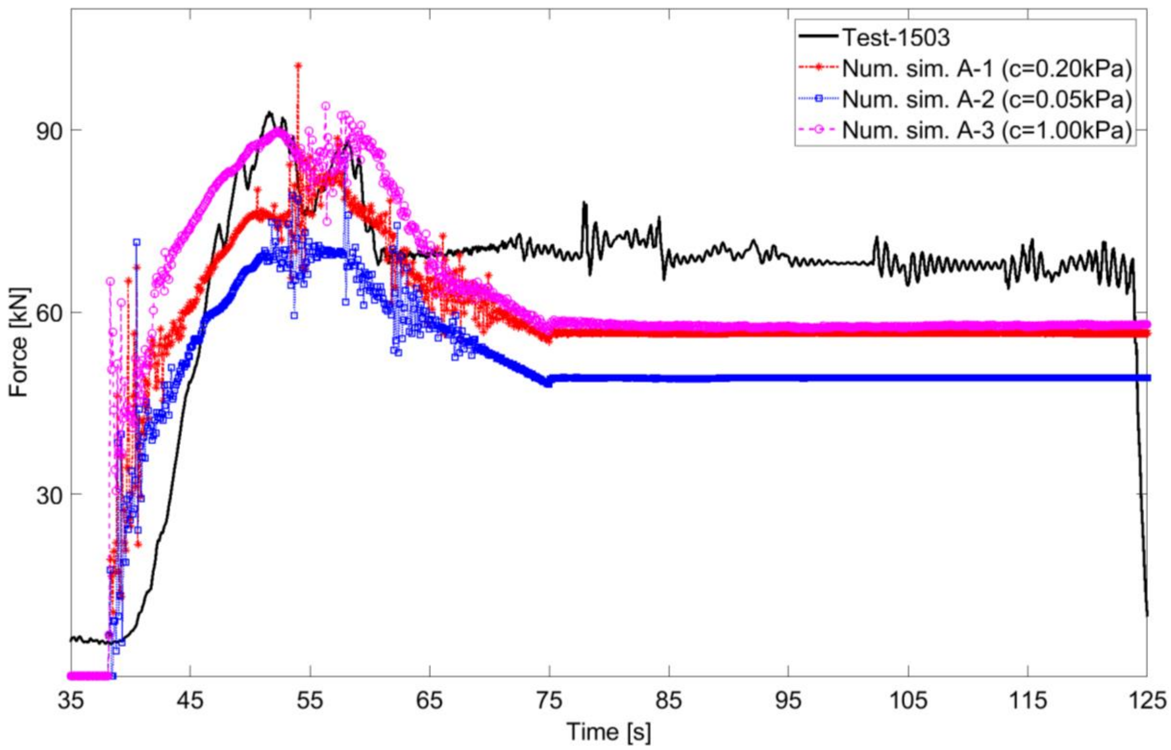


Fig. 12. Comparison of cohesion (c) ($V_f$ =70%, φ=50)

In simulation B-1, B-2 and B-3 cohesion values of 0.2kPa, 0.05kPa and 1kPa were used respectively. As the cohesion value increases, higher force was needed to lift the same amount of brash ice blocks. For all the simulations in series A, the predicted residual forces were lower than measured one. In Fig. 13, the simulation B-3 registered the highest force, which also has the highest cohesion in that series. Therefore, it again indicates that the force required to lift brash ice mass is proportional to cohesion.

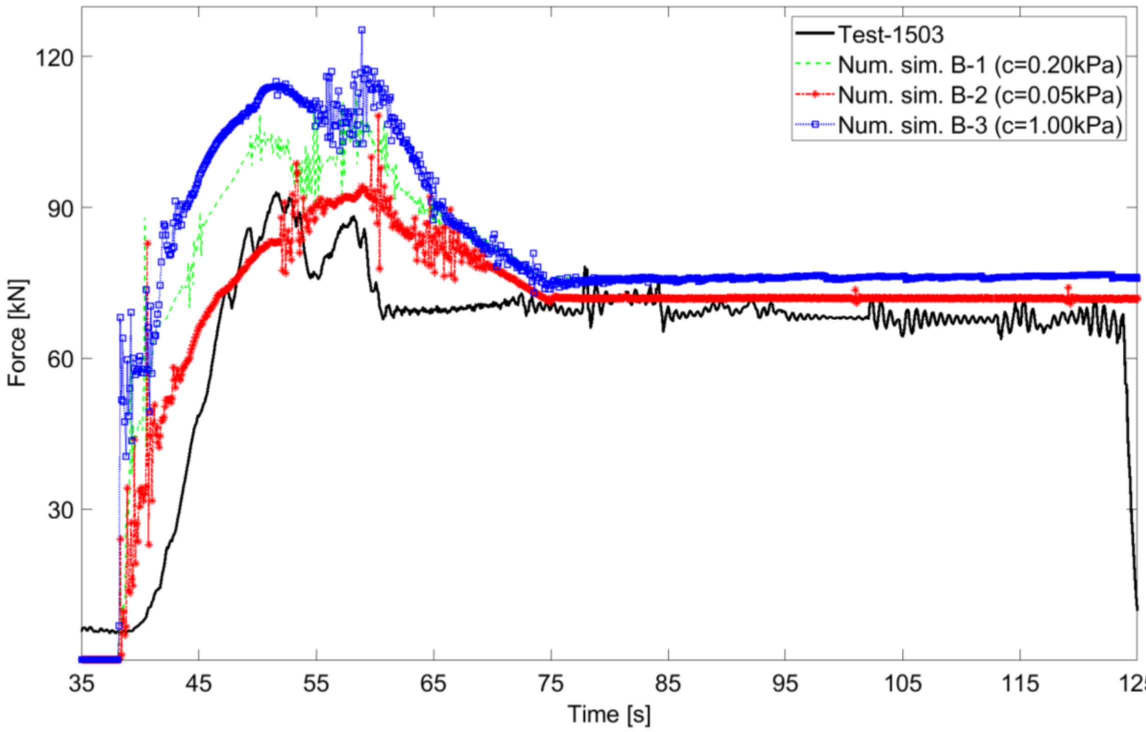


Fig. 13. Comparison of cohesion (c) ($V_f$ =60%, φ=50)

The ice blocks movement, failure mode and plug formation in simulation showed similarities to that experimentally observed one. As the simulation progresses, particles are pushed into the cavity formed by the collector, then later the plug shape narrowed down. Finally, a constant force level was achieved as the collector was above the rest of brash ice layer. Neighbouring particles quickly filled the hole created by collector. This trend was observed in all simulation series with varying peak and residual forces.

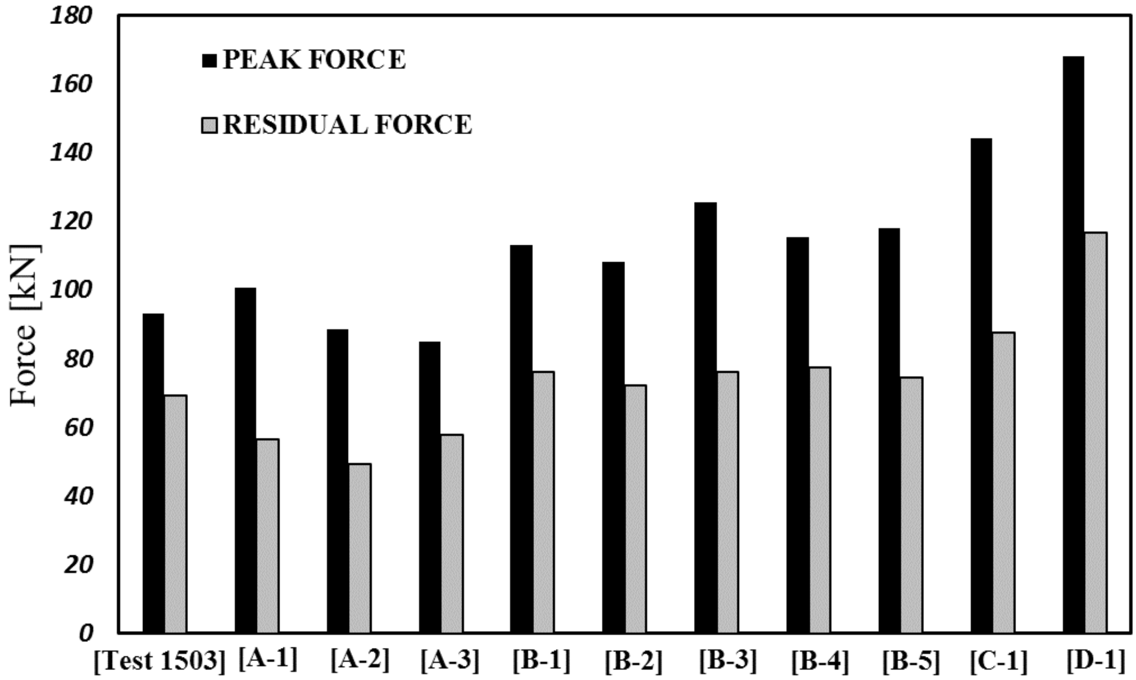


Fig. 14. The peak force and residual force for test and each simulation.

To compare the measured peak ($F_{peak}$) and residual ($F_{res}$) force to simulated forces, a bar chart is plotted, see in Fig. 14. The test data was plotted at the left side of the chart, which can be compared to all simulation data. Based only on values of peak and residual force, numerical simulation B-1 and B-2 were the closest matches. All of the simulations have registered smaller peak forces, suggesting that there is an initial force required to start the movement of the collector. To shows the deformation of brash ice at different times during the simulation, snapshots are given in Fig. 15. After a 5 sec into simulation, a bulge was formed at the top surface of the SPH brash ice field, see Fig. 15 (a). Then the plug formation process started. First a wider plug was formed, see Fig. 15 (b), followed by a transformation into a conical shaped plug, see Fig. 15 (c). The final shape of plug was revealed at about 40 sec, see Fig. 15 (d). The hole created by collector was filled by neighbouring particles. In this simulation few particles which were at the edge of the collector were fallen off during final plug shape formation i.e. interval between (c) and (d)

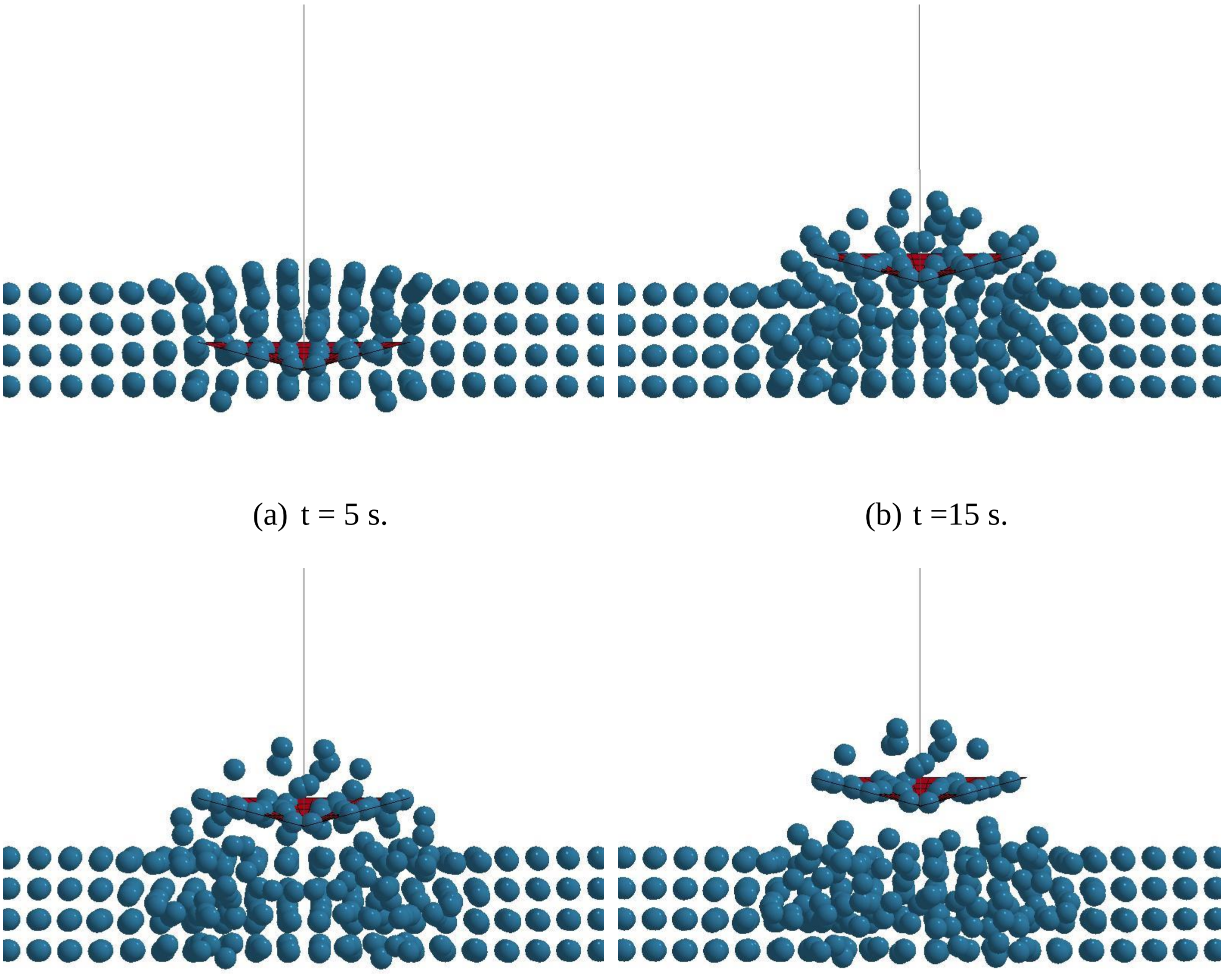

(a) t = 5 s. (b) t =15 s.

(c) t =25 s. (d) t = 40 s.

Fig. 15.Screenshots of simulation of brash ice deformation.

## 7. Discussion

An attempt was made to test brash ice properties using a pull-up test. The test setup performed good enough. However, earlier unsuccessful attempts highlighted the weakness of test mechanism. Also, the issue of test repeatability and no. of test data points, suggests that this study requires more investigation. The ice block shape and size are limiting factors to the effectiveness of this test equipment. The brash ice field where ice block sizes are more than 1 meter cannot be tested with this method. Factors such as the movement of ship and speed of pulling by crane may introduce some errors. Therefore, conducting the test under calm and stable conditions is essential for obtaining accurate results. The test results such as the force-time graph provide valuable input for the validation of a numerical model. Despite the drawbacks of the test methodology, the strength of brash ice was estimated from the force-time graph, on-site observations, and the deformation pattern. The maximum recorded force depends on the breakage of the freeze bonds (if any), friction between the blocks, and weight of the ice blocks. Furthermore, at the beginning of the test, an area larger than the collector was moved. This indicates that ice blocks in brash ice field are interlocked causing an upward-expanding plug. Friction between, and rearrangement of, the ice blocks constitute the dominant processes during pulling of the collector. The test force vs. time plot (Fig. 3) shows that, after an initial peak force there was a subsequent peak force followed by an almost constant residual force. It was observed that two large blocks about 1 m diameter which were at the edge of the collector, fell off after first peak (~55sec). Due to uniform particle spacing, it is not possible to simulate that kind of rearrangement of blocks by this simulation method. This might result in higher residual forces than were observed experimentally.

The SPH method was shown to be useful in simulating large displacement of ice blocks in the pull-up test. It has been shown that, the discrete mass-spring-dash pot model can be used to simulate buoyancy and drag. The strength of the brash ice field can be estimated based on the peak force and certain assumptions of the plug volume. The scaling formulae, based on void fraction, gave reasonable values for the elastic modulus, fracture toughness and fracture energy of a brash ice field. The yield surface parameters $\alpha$ and $\theta$, were estimated based on their relationship to the Mohr-Coulomb criterion. All other yield surface input parameters in CSCM were based on recommendations given in Murray et al. (2007). A parametric study was conducted to see the effect of void fraction, cohesion and internal friction angle. This parametric study shows that simulation B-1 which has 60% void fraction with a cohesion of 0.2kPa and angle of internal friction of 50°, give the overall best fit to the measured force time curve. Fig. 15 shows the deformation of brash ice blocks at different times of the simulation B-1. Due to uneven movement of the pole in the X-Y plane, a non-uniform plug was formed during the simulation which coincided with the test observations.

The discrepancies between the simulated and measured force time series indicate the need for further fine tuning of the numerical and assumed material model parameters. It is worth mentioning that the physical background of the parameters (such as elastic modulus, fracture energy, etc.) should be further investigated in view of brash ice deformation. In current study, some of the parameters to define the shape of failure envelope were selected based on recommended values. However, the numerical model was able to capture different deformation patterns such as a plug that was wider than the collector and filling of a hole quickly with neighbouring particles. The simulation of the brash ice failure process corresponded realistically to the full-scale field observations. The numerical results obtained were able to capture the general trend of brash ice behaviour in the test. This study can be basis to future investigation of brash ice deformation and development of numerical model.

## 8. Summary and conclusions

In this paper, the results of a novel test for brash ice field were presented. The results were interpreted and used to estimate brash ice field properties. The same test was numerically simulated using SPH method and CSCM as material model for brash ice. The test equipment functioned generally good enough, but some weaknesses and limitations of the test equipment were identified. However, efforts were devoted to understanding the physics behind the deformation behaviour of the brash ice field. The presented SPH model gives the opportunity to study the brash ice structure interaction in realistic boundary condition. Modelling brash ice with CSCM presents both opportunities and challenges. Finding suitable input parameters for CSCM can be a time-consuming task. The presented model of the brash ice field, with some modifications, can be used to simulate the ship brash ice interaction. Based on results of the test and numerical simulations, the following conclusions are drawn:

1. The collector arm folding mechanism was found be crucial for workings of the test setup.
2. Future testing must include on site measurement of void ratio and ice blocks size distribution.
3. The presented test method can be employed in laboratories, where environmental parameters such as pulling speed and stable platform can be more closely controlled.
4. The CSCM has the capability of capturing different failure modes of the brash ice such as compaction and dilation under loading but further experimental investigation is needed on material model parameters. The procedure to calibrate CSCM particles require extensive sets of experimental data such as tri-axial compression, tension and shear strength and fracture toughness tests. The absence of such experimental data requires to rely on assumptions.
5. The scaling formula used to estimate brash ice field properties, is based on linear scaling factor of $\left(1-\sqrt{V_f}\right)$. The depth-dependent brash ice field properties cannot be scaled with this formula. Therefore, more investigation is needed to find appropriate scaling formula.
6. The presented SPH model, with the discrete mass-spring-dashpot model to simulate buoyancy and drag, has potential to simulate ship-brash ice interaction. Thus, this representation of the brash ice field can be further developed to estimate the resistance to shipping in brash ice fields.
7. With moderate success, the numerical simulations have captured the behaviour of brash ice in brash ice field.

**Acknowledgement**

The authors gratefully acknowledge the financial and technical support from the Research Council of Norway, (project number 195153, ColdTech) and industrial partners. The project group of SSPA Sweden AB, the crew of the tugboat 'Viscaria' and the staff of the Port of Luleå are thanked for their support. Special thanks to Dr. Ross Wakelin (SINTEF Narvik) for his intensive proofreading of this paper.

**Data Availability Statement**

c. Some or all data, models, or code that support the findings of this study are available from the corresponding author upon reasonable request.

**References**

Bonath, V., Petrich, C., Patil, A., Fransson, L., and Cwirzen, A. (2020). "Seasonal development and resistance of a regularly broken ice-covered ship channel in the Baltic Sea." *Cold Regions Science and Technology*.

Bonath, V., Zhaka, V., and Sand, B. "Field measurements on the behavior of brash ice." *Proc., Proceedings of the 25th International Conference on Port and Ocean Engineering under Arctic Conditions*.

Cabrera, M. I. (2017). "Smoothed particle hydrodynamics modeling of brash ice." Advance Master in Naval Architeture Master Thesis, University of Liege, University of Rostock.

Dobrodeev, A. A., and Sazonov, K. E. "Ice resistance calculation method for a ship sailing via brash ice channel." *Proc., Proceedings of the 25th International Conference on Port and Ocean Engineering under Arctic Conditions*.

Ettema, R., Matsuishi, M., and Kitazawa, T. (1986). "Model tests on ice-rubble size and ship resistance in ice rubble." *Cold Regions Science and Technology*, 12(3), 229-243.

Ettema, R., Schaefer, J., and Huang, H. (1998). "Ice-tank data on brash-ice loads against barges." *Journal of cold regions engineering*, 12(3), 153-161.

Fransson, L., and Sandkvist, J. "Brash ice shear properties : laboratory tests." *Proc., The 8th International Conference on Port and Ocean Engineering Under Arctic Conditions : proceedings* Dansk hydraulisk institut.

Fransson, L., and Stehn, L. "Porosity effects on measured strength of warm ice." *Proc., Proceedings of the 12th International Conference on Port and Ocean Engineering under Arctic Conditions (POAC)*, 17-20.

Gingold, R. A., and Monaghan, J. J. (1977). "Smoothed particle hydrodynamics: theory and application to non-spherical stars." *Monthly notices of the royal astronomical society*, 181(3), 375-389.

Greisman, P. (1981). "Brash Ice Behavior." COAST GUARD RESEARCH AND DEVELOPMENT CENTER GROTON CT.

Greisman, P. (1981). "Brash ice behaviour." United States Coast Guard, Research And Development Center, Avery Point, Groton, Connecticut 06340.

Heinonen, J. (2004). "Constitutive modeling of ice rubble in first-year ridge keel."PhD, Helsinki University of Technology Espoo, Finland.

Hopkins, M. A., Hibler III, W., and Flato, G. (1991). "On the numerical simulation of the sea ice ridging process." *Journal of Geophysical Research: Oceans*, 96(C3), 4809-4820.

Hopkins, M. A., Tuhkuri, J., and Lensu, M. (1999). "Rafting and ridging of thin ice sheets." *Journal of Geophysical Research: Oceans*, 104(C6), 13605-13613.

Hu, J., and Zhou, L. (2015). "Experimental and numerical study on ice resistance for icebreaking vessels." *International Journal of Naval Architecture and Ocean Engineering*, 7(3), 626-639.

ISO19906 (2010). "Petroleum and natural gas industries - Arctic offshore structures."

Jeong, S.-Y., Jang, J., Kang, K.-J., and Kim, H.-S. (2017). "Implementation of ship performance test in brash ice channel." *Ocean Engineering*, 140, 57-65.

Keinonen, A., and Nyman, T. "An experimental model-scale study on the compressible, frictional and cohesive behaviour of broken ice mass." *Proc., Proc. of the Int. Symp. on Ice. Lulea, Sweden*, 335-353.

Kim, J.-H., Kim, Y., Kim, H.-S., and Jeong, S.-Y. (2019). "Numerical simulation of ice impacts on ship hulls in broken ice fields." *Ocean Engineering*, 180, 162-174.

Kitazawa, T., and Ettema, R. (1985). "Resistance to ship-hull motion through brash ice." *Cold Regions Science and Technology*, 10(3), 219-234.

Korzani, M. G., Galindo-Torres, S. A., Scheuermann, A., and Williams, D. J. (2017). "Parametric study on smoothed particle hydrodynamics for accurate determination of drag coefficient for a circular cylinder." *Water Science and Engineering*, 10(2), 143-153.

Li, F., Kõrgesaar, M., Kujala, P., and Goerlandt, F. (2020). "Finite element based meta-modeling of ship-ice interaction at shoulder and midship areas for ship performance simulation." *Marine Structures*, 71, 102736.

Liu, G.-R., and Liu, M. B. (2003). *Smoothed particle hydrodynamics: a meshfree particle method*, World scientific.

LS-DYNAa (2017). "LS-DYNA Keyword User's Manual, Volume I, R10.0."

Lucy, L. B. (1977). "A numerical approach to the testing of the fission hypothesis." *The astronomical journal*, 82, 1013-1024.

Luo, W., Jiang, D., Wu, T., Guo, C., Wang, C., Deng, R., and Dai, S. (2020). "Numerical simulation of an ice-strengthened bulk carrier in brash ice channel." *Ocean Engineering*, 196, 106830.

Matala, R., and Skogström, T. "Soil mechanics measurement methods applied in model brash ice." *Proc., Proceedings of the 25th International Conference onPort and Ocean Engineering under Arctic Conditions*.

Melia, N., Haines, K., and Hawkins, E. (2016). "Sea ice decline and 21st century trans-Arctic shipping routes." *Geophysical Research Letters*, 43(18), 9720-9728.

Mellor, M. (1980). "Ship resistance in thick brash ice." *Cold Regions Science and Technology*, 3(4), 305-321.

Monaghan, J. J. (1994). "Simulating free surface flows with SPH." *Journal of computational physics*, 110(2), 399-406.

Monaghan, J. J. (2005). "Smoothed particle hydrodynamics." *Reports on progress in physics*, 68(8), 1703.

Murray, Y. D. (2007). "Users manual for LS-DYNA concrete material model 159." United States. Federal Highway Administration. Office of Research ….

Murray, Y. D., Abu-Odeh, A. Y., and Bligh, R. P. (2007). "Evaluation of LS-DYNA concrete material model 159."

Patil, A., Sand, B., and Fransson, L. (2015). "Finite element simulation of punch through test using a continuous surface cap model." *Proceedings of the 23nd International Conference on Port and Ocean Engineering under Arctic Conditions*Trondheim, Norway.
Patil, A., Sand, B., and Fransson, L. "Smoothed particle hydrodynamics and continuous surface cap model to simulate ice rubble in punch through test." *Proc., Proceedings of the 23nd International Conference on Port and Ocean Engineering under Arctic Conditions June 14-18, 2015 Trondheim, Norway*.
Polojarvi, A., and Tuhkuri, J. (2009). "3D discrete numerical modelling of ridge keel punch through tests." *Cold Regions Science and Technology*, 56(1), 18-29.
Polojärvi, A., and Tuhkuri, J. (2013). "On modeling cohesive ridge keel punch through tests with a combined finite-discrete element method." *Cold regions science and technology*, 85, 191-205.
Polojärvi, A., Tuhkuri, J., and Korkalo, O. (2012). "Comparison and analysis of experimental and virtual laboratory scale punch through tests." *Cold regions science and technology*, 81, 11-25.
Prodanovic, A. "Model tests of ice rubble strength." *Proc., Port and ocen engineering under arctic conditions*.
Riska, K., Bridges, R., Shumovskiy, S., Thomas, C., Coche, E., Bonath, V., Tobie, A., Chomatas, K., and de Oliveira, R. C. D. (2019). "Brash ice growth model–development and validation." *Cold Regions Science and Technology*, 157, 30-41.
Robb, D. M., Gaskin, S. J., and Marongiu, J.-C. (2016). "SPH-DEM model for free-surface flows containing solids applied to river ice jams." *Journal of Hydraulic Research*, 54(1), 27-40.
Sandkvist, J. (1978). *Problems in keeping year-round navigation in the Luleå harbour*, Division of Water Resources Engineering, University of Luleå, Sweden.
Sandler, I. S., Dimaggio, F. L., and Baladi, G. Y. (1976). "Generalized cap model for geological materials." *Journal of Geotechnical and Geoenvironmental Engineering*, 102(ASCE# 12243 Proceeding).
Schwer, L. E., and Murray, Y. D. (1994). "A three-invariant smooth cap model with mixed hardening." *International Journal for Numerical and Analytical Methods in Geomechanics*, 18(10), 657-688.
Schwer, L. E., and Murray, Y. D. "Continuous surface cap model for geomaterial modeling: a new LS-DYNA material type." *Proc., Seventh International LSDYNA Users Conference. Dearborn. Michigan, LSTC& ETA*, 16-35.
Simo, J. C., and Ju, J. (1987). "Strain-and stress-based continuum damage models—I. Formulation." *International journal of solids and structures*, 23(7), 821-840.
Sorsimo, A., Nyman, T., and Heinonen, J. (2014). "Ship-Ice Interaction in a channel." H. Winter Navigation Research Board, ed.
Sukhorukov, S., and Løset, S. (2013). "Friction of sea ice on sea ice." *Cold Regions Science and Technology*, 94, 1-12.
Swegle, J., Hicks, D., and Attaway, S. (1995). "Smoothed particle hydrodynamics stability analysis." *Journal of computational physics*, 116(1), 123-134.
Tatinclaux, J., Lee, C., Wang, T., Nakato, T., and Kennedy, J. (1976). "A laboratory investigation of the mechanics and hydraulics of river ice jams." Iowa Institute of hydraluic Research, Iowa city, Iowa, 45.
Tatinclaux, J., Lee, C., Wang, T., Nakato, T., and Kennedy, J. (1976). "A laboratory investigation of the mechanics and hydraulics of river ice jams." IOWA INST OF HYDRAULIC RESEARCH IOWA CITY.
Trafi (2010). "Finnish-Swedish Ice Class Rules 2010." Finnish Transport Safety Agency.

Tran, T. T. (2018). "Study of the SPH Method for Simulation in LS-DYNA." *Study of the SPH Method for Simulation in LS-DYNA*, 7(8), 271-274.
Weeks, W. (2010). *On sea ice*, University of Alaska Press.
Xu, J., and Wang, J. "Interaction methods for the SPH parts (multiphase flows, solid bodies) in LS-DYNA." *Proc., Proceedings of the 13th International LS-DYNA Users Conference, Detroit, MI, USA*, 8-10.
Yreux, E. (2018). "Fluid Flow Modeling with SPH in LS-DYNA®."
Zhang, N., Zheng, X., Ma, Q., and Hu, Z. (2019). "A numerical study on ice failure process and ice-ship interactions by Smoothed Particle Hydrodynamics." *International Journal of Naval Architecture and Ocean Engineering*, 11(2), 796-808.